



Published in final edited form as:

J Neural Eng.; 17(1): 016031. doi:10.1088/1741-2552/ab4104.

Spinal cord neural interfacing in common marmosets (*Callithrix jacchus*)

Noeline W Prins¹, Ramanamurthy Mylavarapu¹, Alden M. Shoup¹, Shubham Debnath¹, Abhishek Prasad^{1,*}

¹Department of Biomedical Engineering, University of Miami, Coral Gables, FL 33146

Abstract

Objective: Spinal cord injury (SCI) remains an ailment with no comprehensive cure, and affected patients suffer from a greatly diminished quality of life. This large population could significantly benefit from prosthetic technologies to replace missing limbs, reanimate nonfunctional limbs, and enable new modes of technologies to restore muscle control and function. While cortically driven brain machine interfaces (BMIs) have achieved great success in interfacing with an external device to restore lost functions, interfacing with the spinal cord can provide an additional site to record motor control signals, which can have its own advantages, albeit challenges from using a smaller non-human primate (NHP) model. The goal of this study is to develop such a spinal cord neural interface to record motor signals from the high cervical levels of the spinal cord in a common marmoset (*Callithrix jacchus*) model.

Approach and Main Results: Detailed methods are discussed for this smaller NHP model that includes behavioral training, surgical methods for electrode placement, connector placement and wire handling, electrode specifications and modifications for accessing high cervical level interneurons and motoneurons. The study also discusses the methods and challenges involved in behavioral multi-channel extracellular recording from the marmoset spinal cord, including the major recording failure mechanisms encountered during the study.

Significance: Marmosets provide a good step between rodent and larger NHP models due to their small size, ease of handling, cognitive abilities, and similarities to other primate motor systems. The study shows the feasibility of recording spinal cord signals and using marmosets as a smaller NHP model in behavioral neuroscience studies. Interfacing with the spinal cord in chronically implanted animals can provide useful information about how motor control signals within the spinal cord are transformed to cause limb movements.

Keywords

Marmosets; Spinal Cord; spinal cord neural interface

After the embargo period, everyone is permitted to use copy and redistribute this article for non-commercial purposes only, provided that they adhere to all the terms of the licence <https://creativecommons.org/licenses/by-nc-nd/3.0>

*Corresponding Author **Abhishek Prasad, PhD**, Department of Biomedical Engineering, University of Miami, 1251 Memorial Dr, MEA 203, Coral Gables, FL 33146, **Phone:** 305-243-4886, a.prasad@miami.edu.

Conflict of Interest:

The authors declare no competing financial interests.

1. Introduction

There are over 2.5 million cases of spinal cord injury (SCI) worldwide with over 250,000 patients just in the United States [1]. SCI remains a global issue and although incidence rates vary between countries, studies indicate a trend of increasing prevalence in recent decades [2]. SCI does not have a comprehensive cure, leads to a significant decline in the patient's quality of life, and factors such as costs of treatments, rehabilitation, and medical expenses place heavy financial burden on the impacted patients and their families [1, 3]. Due to the injury, the descending signal pathways carrying voluntary command signals from the brain lose their connections with the spinal cord circuitry below the level of the injury and result in the loss of movement and function. Neural prosthetics, when introduced into activities of a patient's day-to-day life, can restore select movements either through the implementation of a robotic limb or using the individual's own limbs through functional electrical stimulation (FES) [4–15]. Current neuroprosthetics research has mainly focused on the use of cortical signals as input to brain-machine interfaces (BMIs) for control of artificial limbs [6, 14, 15], computer cursors [11, 13], and muscles through FES [4, 5, 10].

Most BMIs have utilized signals from relevant cortical sites involved in motor planning and movement generation including the primary motor, premotor, and parietal areas of the cortex [16–34]. It is understood, however, that cortical signals undergo further processing prior to their use in muscle activation [35, 36]. Spinal neurons consolidate descending motor information from cortical and subcortical structures and convert them into specific motor commands suitable for causing muscle movements; this integration of information at the level of the spinal cord is mediated by an extensive network of interneurons and propriospinal neurons [37]. Among these spinal networks, studies have found neurons in the high cervical levels contain motor commands for forelimb reaching movements, where the interneurons and the propriospinal neurons at the C3-C4 level mediate forelimb target reaching, grasping, and precision grip [38–41]. The C3-C4 neurons not only mediate target reaching but also updates the descending motor commands from the cortex for trajectory updating and deceleration in case of environmental perturbations [42, 43]. Presence of such converging information, its relationship to forelimb movement generation, and the presence of inhibitory input from segmental interneurons that allows for feedback from musculature [38–44] makes the C3-C4 cervical spinal cord an interesting target for neural interfacing studies. These studies provide the rationale for using the spinal cord as a point of convergence for recording motor signals from supraspinal structures that can potentially be used as control signals in a neuroprosthetic approach.

The feasibility for such an approach to access signals from the spinal cord requires proof-of-concept evaluation in various animal models such as rodents and nonhuman primates (NHP) such as those shown for cortically driven BMIs [23, 32, 45–47]. In this study, we used a smaller non-human primate (NHP) model, common marmoset (*Callithrix jacchus*) that is increasingly being used in neuroscience research [48–50]. Marmosets provide a good step between rodent and larger NHP models for behavioral neuroscience studies due to their small size, ease of handling, cognitive abilities, and similarities to other primate motor systems [49–52]. The goal of this study is to discuss detailed methods that are necessary to create a spinal cord neural interface in common marmosets. We discuss our experience in

working with this animal model that includes behavioral training and performing chronic recordings from awake behaving animals. We also discuss in detail the microelectrode array specifications and design modifications suited for interfacing with the spinal cord and surgical techniques for microelectrode placement in the marmoset spinal cord.

2. Methods and Results

Five adult male marmosets were used in this study. Table 1 includes a summary of all the animals used in the study, their recording duration post-surgery, and the cause of recording failure. All animal care, surgical, and research procedures were performed in accordance with the National Research Council Guide for the Care and Use of Laboratory Animals and was approved by the University of Miami Institutional Animal Care and Use Committee (IACUC).

2.1. Electrode Arrays

Figure 1 shows the schematics of the microelectrode array used in the study and its intended implant location relative to the spinal cord tissue (Figures 1A–1C). Platinum-iridium (Pt-Ir) floating microelectrode arrays (FMA, MicroProbes for Life Science, Gaithersburg, MD) were used (Figures 1D and 1E). FMAs were either 13 channel (1D) or 32 channel (1E), made up of three or four rows of electrodes with 250 μm separation and consisted of a 4–5 cm cable from the array to the connector. A silicone sheath was used for reinforcing the wire from the connector to the array (1E). All MEAs were sterilized using ethylene oxide (EtO) gas in a gas sterilizer prior to surgery.

2.2. Surgical Procedure

2.2.1 Animal preparation and physiological vitals measurements: All surgical procedures were performed in a dedicated surgical suite under sterile conditions. Animals were fasted for up to 12 hours prior to surgery to minimize risk of pulmonary aspiration during administration of anesthesia. Animals were anesthetized with ketamine (intramuscular, 10–50 mg/kg) and aseptically prepped for surgery. Upon shaving the surgical site (head and the back), the animals were maintained under deep anesthesia using isoflurane (0.5–4%) and oxygen (1–2L/min) delivered through a nose cone attached to the stereotaxic apparatus. Their vital measurements, which included rectal temperature, heart rate, electrocardiogram (ECG), and peripheral capillary oxygen saturation (SpO₂) were continuously monitored. Additionally, blood glucose was periodically monitored during the surgical procedure.

2.2.2 Skull preparation for headstage assembly: The animals were positioned with appropriate ear and bite bars on a standard stereotaxic frame (Kopf Instruments, Tujunga, CA) for small animals. Eye lube was applied on the eyes. The animals were then draped with sterile drapes and the head and upper back were cleaned with multiple scrubs of iodine and isopropyl alcohol. A dorsal midline incision was made on the skull and the periosteum was removed to expose the skull surface. Appropriate drill bits corresponding to the size of the anchoring screws were used to manually drill holes on the skull. Care was taken to ensure that the holes did not extend beyond the skull into the cranial space. Four to six

screws (00–90 gauge) were then manually inserted into the predetermined locations (Figure 2Ai). These screws were used as an anchor for the array connector. The FMA connector was then fixed on the skull using dental acrylic.

2.2.3 Laminectomy: Following screw placement and fixing the connector on the skull, the bony protrusion of the spinous process at the second cervical vertebrae C2 was identified on the animal's back as this spinous process is palpable over the skin. A midline incision was made from the base of the skull to the thoracic vertebrae and the skin was retracted to expose the back muscles. A pair of blunt-tipped scissors were used to separate the muscles under the incision site to expose the cervical vertebrae C2–C7. Subsequently, a laminectomy was performed at the C3–C4 level of the spinal cord ipsilateral to the dominant arm. Figure 2A(i) shows the laminectomy at the C3–C4 level. In the first animal, two screws, similar to the skull screws, were drilled in the C2 and C5 vertebra, with the assumption that these screws will stabilize the spinal cord where the FMA would eventually be implanted. We did not observe any advantage associated with placing the screws on the vertebrae and therefore, chose not to place screws on the vertebrae in the other animals. This also reduced the overall surgical time and the additional surgical risk associated with drilling screws into the vertebrae. Post-mortem analysis in all animals indicated that the FMA was still anchored in the spinal tissue. We also observed in all animals that there was a layer of fibrous tissue that covered the substrate of the FMA that would stabilize the array in the spinal cord tissue, eliminating the need for anchoring screws on the vertebrae.

2.2.4 FMA implantation: Following the laminectomy, the dura was gently lifted with forceps and punctured using a 25-gauge sterile needle bent at approximately 90 degrees. The dura was carefully resected using microscissors to expose the spinal cord. The FMA ceramic substrate was held to a vacuum wand attached to the anterior-posterior (AP) and the medial-lateral (ML) arms of the stereotaxic arm, allowing for accurate positioning of the FMA on one half of the spinal cord in the rostrocaudal axis above the implant location, that corresponded to the laminectomy at the C3–C4 level (Figure 2A(ii)). The MEA was positioned in this manner so that the electrode shanks can span the grey matter along the medial-lateral axis to target the interneuronal and propriospinal circuitry at the C3–C4 level (Figure 1C). A micropositioner (FHC, VT) was used to lower the array assembly slowly (~1mm/minute) into the spinal cord to the desired implant location (Figure 2A(iii)). Figure 2A(iii) shows a close-up of a 32 channel FMA implanted in the C3–C4 segment of the spinal cord. A small piece of gelfoam soaked in sterile saline was then placed on top of the FMA along with a drop of butyl cyanoacrylate (Vetbond, WPI, FL), and a suture at a distant location relative to the implant was placed on the interconnect wire of the FMA to allow for strain relief. The muscles of the back were closed in layers using size 5.0 absorbable sutures, and the skin of the back was closed using size 4.0 absorbable sutures. On the skull, more acrylic was applied in layers around the FMA connector (Figure 2A(iv)) to encase it securely. Care was taken to avoid putting any dental acrylic where the interconnect wire exited the micro-connector, allowing the wire assembly to remain flexible when the animals made head movements.

2.2.5 Intraoperative and chronic electrophysiological recordings:

Electrophysiological recordings were performed concurrently with FMA insertion into the spinal cord. Spinal cord signals were recorded at 24,414 Hz sampling rate and bandpass filtered between 500–6000 Hz using a real-time data acquisition system (RZ2, TDT, FL) while inserting the FMA through the spinal cord tissue. Online spike sorting based on manually set thresholds and box sorts were used to isolate spiking activity. Figure 2B shows an example of multi-unit activity from the spinal cord obtained intraoperatively after the FMA was inserted into the cord at the target location. Intraoperative electrophysiological recording was useful in guiding the eventual placement of the array at the desired location and depth. Figure 2C shows examples of four channels of broad band activity (bandpass filtered between 500Hz-6kHz) from the spinal cord on day 0 (day of implant) and at two chronic time-points (day 35 and day 98).

2.3. Post-operative recovery and care

Postoperative care entailed monitoring of cardiac stability, glucose, and temperature. Animals generally were awake within 15–30 minutes after anesthesia removal. They were returned to their home cages once they regained consciousness and regained sufficient mobility. Animals were monitored daily for neurological markers such as nystagmus, alertness, grip and limb strength, gait, and climbing ability. Further, special attention was given to the animal's diet, hydration, and solid waste excretion in the days post-surgery. During this time, they were more frequently offered treats, rice milk, and a nutrition drink (Ensure, Abbott Labs, USA) to aid recovery. After surgery, implanted animals were single housed to prevent other animals from interfering with the surgical wound. Cephalixin (20mg/kg orally twice daily for 5 days) and buprenorphine (0.001–0.015mg/kg IM twice daily for 3 days) were administered as an oral antibiotic and an analgesic, respectively.

Post-surgery, animals were monitored for signs of pain and distress such as lethargy, over-grooming or scratching excessively, self-mutilation, shaking, reluctance to eat, drink, or swallow, abnormal or hunched posture, guarding, urine, stool consistency, and signs of dehydration. Animals were also monitored for neurological indications such as abnormal posture of head and neck, nystagmus, abnormal gait, paralysis, forelimb movements and range of motion, grip strength, and climbing capability, as a result of electrode placement in the spinal cord tissue. Neurological deficits in the forelimbs can occur due to the placement of the microelectrode array in the spinal tissue that control forelimb movements. Post-surgery, though animals tended to favor the use of their contralateral arm for reaching and grasping, they used all four limbs for weight bearing and climbing. Grip strength was reduced in the ipsilateral arm post-operatively, but all animals recovered within 2–3 weeks following surgery. At these time points, their grip strength improved, and they tended to use both limbs in daily activities.

Marmosets are arboreal animals and spend a significant amount of time on top of the cage and climbing around. In our experience, microelectrode implantation did not cause paralysis in the limbs of any of the implanted animals. There were also no behavioral changes in the animals. We used micro computed tomography (micro-CT) images to evaluate if there was any indication of loss of spinal tissue and compression of the spinal cord as a result of the

implant and the microelectrode array substrate. Micro-CT was performed after the animals were euthanized and the spinal cord harboring the electrode was dissected out. Figure 3A shows a brightfield image of an intact marmoset spinal cord with no implant at the C3-C4 level. Figure 3B is a micro-CT image with the microelectrode implant in the spinal cord. The dense tissue around the array is the spinal tissue. Clearer, higher resolution images could not be obtained because of low resolution of the scanner, contrast issues between the tissue and highly reflective metal electrodes, and the small size of the tissue being imaged. However, it can be observed that the microelectrode array did not appear to cause a loss of tissue around the electrode tips and the array also did not compress the spinal cord tissue at the dorsal surface where it penetrated the tissue. Figure 3C shows the micro-CT image overlaid on the brightfield image of an unimplanted cord to visualize the location of the electrode tips relative to the spinal cord.

2.4. Behavioral Task

Animals were not food or water deprived for behavioral training. Prior to training for any of the behavioral tasks, animals received basic scoop and chair training. Subsequently, the animals were trained to complete reaches for one of three types of tasks: a nine-target reaching task (Figure 4A), two-target robot task and a touch screen task. For the nine-target reaching task, the sequence of the trial is shown in Figure 4B with the experimental timeline. During each session, the animal sat in front of the custom-made behavioral device with the door closed. Each trial was initiated by the experimenter, with the animal placing his hand on an infrared sensor (touchpad) for a random hold period (700–1200 msec). After the random hold period, an audio cue ('Go Tone') was presented simultaneously with the door opening, revealing a treat at one of the 9 targets. The animals had to reach, grasp, and retrieve the food accurately within 2 seconds before the door was closed again. For the two-target robot task, the timing and trial information was the same. However, instead of reaching to a treat, the animal reached to a sensor indicated by a light either on the left or right and successfully captured targets resulted in robot movement and a treat [47]. In the touchscreen task, a target appeared on the screen and the animal was required to trigger the target within a 2 seconds period. Animals were considered to be trained for a particular task if they were able to perform the task with at least 80% accuracy. Table 1 summarizes the approximate number of trials each animal performed during each session, the recording duration post-surgery, and the cause of the recording failure. Table 1 also gives the trials per session once the animal was fully trained. Figure 4C shows the training time it took for each animal for reaching different behavioral milestones before surgery, the average duration for all animals is shown in 4D, and the approximate time that each animal spent on the behavioral chair performing the task during each session is shown in Figure 4E. In general, once the animals had kinematic tracking markers and surgical procedure done, the average number of trials per session for all animals reduced to about 20–60 trials per session.

We defined each of the milestones during the behavioral training as the following in the order they were introduced to the animals:

Scoop Training: Animals were transferred between the home cage and the experimental chair using a custom-made scoop [49], and were considered trained when they were

comfortable with getting into the scoop within five minutes. Four of the five animals were scoop trained in 5–6 days while the last animal took approximately two weeks (Figure 4C).

Chair Training: An animal was considered chair trained if the animal was comfortable sitting in chair and was not agitated or vocalizing for at least 15 min. All five animals were chair trained in 1–2 weeks.

Free Reach: Animals were considered trained for free reaching when they learned to reach for food treats with their hands instead of reaching with their mouth or tongue. Once calm in a seated position in the chair, the animals learned to reach freely in less than a week.

Touchpad training: Trials were time aligned with the use of an infrared sensor attached to a touchpad. The animals were “touchpad trained” when they successfully kept their hand on the touchpad for the random hold period. This part of the training took the longest time where some animals were able to learn faster than others (~1.5–5.7 weeks).

Reaching Task: Animals were considered trained for the reaching tasks when they willingly reached to all required target locations to receive food rewards. All animals learned this within two weeks.

2.5. Kinematics Acquisition

Forelimb kinematics during the reaching tasks were acquired using 2 different systems. One system consisted of four infrared cameras (Innovision Systems, Columbiaville, MI) positioned around the animal to capture forelimb movements sampled at 60 Hz. Two spherical infrared sensors were attached to velcro and placed on the animal’s forelimb at the forearm and wrist to track the forelimb kinematics. Kinematic information was streamed at 60 frames per second to the MaxPRO software (Innovision Systems, Columbiaville, MI). The frames were tracked offline following the recording sessions and three-dimensional trajectory data from each marker was exported into MATLAB for further analysis. The second system was a 3D tracking system by Trakstar (Ascension technologies, Shelburne, VT) sampled at 1017 Hz. It consisted of a sensor attached to the animal’s hand and a magnetic field generated by a DC magnetic field transmitter. Figure 5A shows example trajectories (x,y and z directions) from two animals during reaching movement. Each subplot is an average of five reaching trials towards one target. Figure 5A(i) is using the MaxPRO system. Figure 5A (ii) shows the data acquired with trackstar system from a different animal. Depending on the task, some animals did not have kinematics tracking, instead only end point information. Figure 5A (i) and (ii) show different x, y and z directions, which is unique to the system the data is recorded from. Figure 5B shows the 3D trajectories for individual reaching trials in two animals. Figure 5B(i) illustrates 3D trajectories in four directions and Figure 5B(ii) illustrates trajectories in two directions. In each instance, movement started at the touchpad, reached one of the visible targets, and ended at the mouth.

2.6 Spinal Cord Recordings

Neural signals were recorded at 24,414 Hz sampling rate and 24-bits of resolution using a real-time data acquisition system (RZ2, TDT, FL) and a custom-made software program

(RPvdsEx, TDT, FL). A band-pass filter (500–6000 Hz) was used to record neural activity. Multi-unit activity was acquired with manually set threshold levels, and waveforms were discriminated online by amplitude and shape using box-sorting methods. Figure 6A shows histograms from two channels each of multiunit activity from two animals which were sorted online during the experiment. Time zero indicates the movement onset. The time-histograms show an increase in neural activity (Figure 6Ai), which coincides with movement in y direction for animal Ky (Figure 5Ai). Similarly, Figure 6A (ii) shows an increase in neural activity during movement in animal Ax. While the time histograms in Figure 6A show the isolated threshold crossings from individual channels that modulated with the reaching task, Figure 6B illustrates band-pass filtered, rectified-averaged neural signals from all 32 channels from two animals during a reaching trial. The envelope of the rectified-averaged signal (black trace) shows an increase in activity following movement onset and then once again following 0.5 seconds during the retrieval phase. Baseline activity prior to reach onset was different between trials and across channels and an increase in activity in the broadband signals before movement onset can be attributed to the animal moving his forelimb to the touchpad and the muscle force that is needed to keep his forelimb until the next cue. The large amplitude artifact, observed in these traces, is due to chewing of food treats.

3. Discussion

Previously, spinal cord recordings have been reported in larger macaque model [35–37, 53, 54] but not in marmosets; a species which is being increasingly used in neuroscience studies as a smaller non-human primate model. Recordings from the spinal cord can provide an additional area within the motor system, other than the motor cortex, where volitional motor signals can be recorded. However, recording from the spinal cord poses several technical challenges compared to recording from the cortex. Further, accessing these recordings sites in a smaller primate model also presents additional challenges. In this work, we discuss the methods and challenges for chronic recording of spinal cord activity using microelectrode arrays in awake, behaving marmosets, which can be useful for research labs interested in this animal model. We also describe the behavioral task, surgical procedure, and present examples of electrophysiological recordings post-implant.

The spinal cord tissue has a small cross-sectional area, and the cord undergoes large amounts of movement during daily activities. Therefore, the choice of array design is significant to maintaining viable recordings. Penetrating FMAs were chosen over flexible surface electrode arrays based on the deeper anatomical location of neurons involved in motor processing in the spinal cord [55, 56]. In the first few implants (2), we used a lower channel count FMA that consisted of 13 recording channels. This choice was based on the assumption that an array of smaller dimensions with limited electrodes (1.6mm x 1.95mm) would cause less trauma to the spinal cord tissue than a larger array. However, this smaller footprint array could only span one segment of the spinal cord. Therefore, in subsequent animals, we decided to use a 32-channel FMA which was larger than the 13-channel FMA. We used an FMA where the array footprint (1.6mm x 2.8 mm) was slightly larger, had a higher number of electrodes, and a geometry that could span most of the C3 and C4 segments as well as access most of the grey matter in one half of the spinal cord in the

mediolateral direction. In each array design (13- or 32-channel), we used three different electrode lengths (1.3mm, 1.4mm, and 1.5mm Figure 1B) in order to target a majority of neurons within the laminae VII-IX. Extra precaution was taken during the laminectomy and opening of the dura so as to not damage the spinal cord. The dura is significantly thinner than at the cortex and the entire procedure was performed carefully under a surgical microscope to prevent damage to the cord surface. Using an array with tapered tips, such as those used in this study, is also recommended as it aids penetration into the spinal tissue. All animals were monitored carefully post-surgery for several days, and postoperative neurologic deficits were not observed in any of the animals that were implanted with either of the FMA type.

The spinal cord is subjected to a variety of torques during daily activities and thus provides additional challenges during the implantation and securing of a chronic penetrating FMA. We chose a floating electrode array because it can move with the cord, minimizing the relative movement between the two structures compared to a fixed array type. We also placed multiple loops within the interconnect wire so that the array is subjected to minimum strain due to the interconnect wire cable. This also prevents the interconnect wire from pulling the array out of the spinal tissue. A majority of electrode array failure in these implants was due to the interconnect wire breaking at the location where it exits the connector fixed to the skull. Earlier array design (Figure 1D) shows an example where there is no reinforcement on the interconnect wire. Due to the array failures resulting from this wire breaking, later array designs added silicone tubing (Figure 1E) or additional silicone layers (Figure 2A (iv)), incorporated by the manufacturer, on the interconnect cable. We are currently using this array design for the spinal implants because the added reinforcement provided by the silicone minimizes the possibility of wire breakage. Further, the placement of the connector on the skull is also important to minimize wire breakage. In earlier implants, the connector was placed closer to the interaural line. However, the wire between the connector and the array broke in most of those implants. In more recent animals, we moved the connector posterior to the interaural line, which puts less stress on the wire between the connector and the array, minimizing wire breakage.

Representative electrophysiological recordings provide evidence that chronic recordings can be performed using FMAs implanted in the spinal cord of awake behaving marmosets. All recordings were performed with respect to a reference electrode, which was a slightly longer electrode shank (1.8 mm) on the FMA compared to recording electrodes. A separate Pt wire tied to a skull screw was used as the ground. In the first animal, where we drilled two screws on the spinal vertebrae, we used one of the screws for grounding the array. However, we did not observe any significant difference in the noise floor level between using a ground screw on the skull or the vertebrae. There is also a higher risk of damaging the spinal cord with screws on the vertebrae. Therefore, we continued to use the skull screw as ground for all subsequent animals. Recordings in awake, behaving animals suggested an increase in neural activity in the spinal cord that was coincident with forelimb movement. Chronic recordings, such as those shown in Figure 2C suggested an increase in noise floor at chronic time-points, however, field potential and multi-unit activity was still discernible at these time-points. The study showed the feasibility of recording spinal cord signals and using marmosets in behavioral neuroscience studies as a smaller non-human primate due to their small size and

similarities to other primate motor systems. While interconnect cable breakage was the most common recording failure mechanism, use of flexible recording arrays and careful attention to the choice of array and cable design, connector placement, and handling of the wire bundle may result in better recording outcomes chronically.

Acknowledgements:

This work was supported by DOD W81XWH-15-0332, and NIH 1DP2EB022357-01. The authors would like to thank the University of Miami, Division of Veterinary Resources (DVR) for the animal care support and Dr. Gaetan Delcroix and the Miami VA Medical Center / GRECC for the use of their microCT instrument.

References

1. Center, N.S.C.I.S., Facts and Figures at a Glance., in Birmingham, Alabama 2018.
2. Furlan JC., et al., Global incidence and prevalence of traumatic spinal cord injury. *Can J Neurol Sci*, 2013 40(4): p. 456–64. [PubMed: 23786727]
3. DeVivo MJ., Causes and costs of spinal cord injury in the United States. *Spinal Cord*, 1997 35(12): p. 809–13. [PubMed: 9429259]
4. Ajiboye AB., et al., Restoration of reaching and grasping movements through brain-controlled muscle stimulation in a person with tetraplegia: a proof-of-concept demonstration. *Lancet*, 2017 389(10081): p. 1821–1830. [PubMed: 28363483]
5. Bouton CE., et al., Restoring cortical control of functional movement in a human with quadriplegia. *Nature*, 2016 533(7602): p. 247. [PubMed: 27074513]
6. Hochberg LR., et al., Neuronal ensemble control of prosthetic devices by a human with tetraplegia. *Nature*, 2006 442(7099): p. 164–171. [PubMed: 16838014]
7. Moritz CT., Perlmutter SI., and Fetz EE., Direct control of paralysed muscles by cortical neurons. *Nature*, 2008 456(7222): p. 639–642. [PubMed: 18923392]
8. Santhanam G., et al., A high-performance brain-computer interface. *Nature*, 2006 442(7099): p. 195–198. [PubMed: 16838020]
9. Schwartz AB., et al., Brain-Controlled Interfaces: Movement Restoration with Neural Prosthetics. *Neuron*, 2006 52(1): p. 205–220. [PubMed: 17015237]
10. Gant K., et al., EEG-controlled functional electrical stimulation for hand opening and closing in chronic complete cervical spinal cord injury. *Biomedical Physics & Engineering Express*, 2018.
11. Schalk G., et al., Two-dimensional movement control using electrocorticographic signals in humans. *Journal of neural engineering*, 2008 5(1): p. 75. [PubMed: 18310813]
12. Collinger JL., et al., High-performance neuroprosthetic control by an individual with tetraplegia. *Lancet*, 2013 381(9866): p. 557–564. [PubMed: 23253623]
13. Simeral JD., et al., Neural control of cursor trajectory and click by a human with tetraplegia 1000 days after implant of an intracortical microelectrode array. *J Neural Eng*, 2011 8(2): p. 025027. [PubMed: 21436513]
14. Hochberg LR., et al., Reach and grasp by people with tetraplegia using a neurally controlled robotic arm. *Nature*, 2012 485(7398): p. 372–5. [PubMed: 22596161]
15. Taylor DM., Tillery SI., and Schwartz AB., Direct cortical control of 3D neuroprosthetic devices. *Science*, 2002 296(5574): p. 1829–32. [PubMed: 12052948]
16. Aflalo T., et al., Decoding motor imagery from the posterior parietal cortex of a tetraplegic human. *Science*, 2015 348(6237): p. 906–910. [PubMed: 25999506]
17. Batista AP., et al., Reference frames for reach planning in macaque dorsal premotor cortex. *J Neurophysiol*, 2007 98(2): p. 966–83. [PubMed: 17581846]
18. Cisek P. and Kalaska JF., Simultaneous encoding of multiple potential reach directions in dorsal premotor cortex. *J Neurophysiol*, 2002 87(2): p. 1149–54. [PubMed: 11826082]
19. Cisek P. and Kalaska JF., Neural correlates of reaching decisions in dorsal premotor cortex: specification of multiple direction choices and final selection of action. *Neuron*, 2005 45(5): p. 801–14. [PubMed: 15748854]

20. Cui H. and Andersen RA., Posterior parietal cortex encodes autonomously selected motor plans. *Neuron*, 2007 56(3): p. 552–559. [PubMed: 17988637]
21. Desmurget M., et al., Role of the posterior parietal cortex in updating reaching movements to a visual target. *Nature Neuroscience*, 1999 2(6): p. 563–567. [PubMed: 10448222]
22. Donoghue JP., et al., Neural discharge and local field potential oscillations in primate motor cortex during voluntary movements. *J Neurophysiol*, 1998 79(1): p. 159–73. [PubMed: 9425187]
23. Georgopoulos AP., et al., On the Relations between the Direction of Two-Dimensional Arm Movements and Cell Discharge in Primate Motor Cortex. *Journal of Neuroscience*, 1982 2(11): p. 1527–1537. [PubMed: 7143039]
24. Georgopoulos AP., Kettner RE., and Schwartz AB., Primate Motor Cortex and Free Arm Movements to Visual Targets in 3-Dimensional Space .2. Coding of the Direction of Movement by a Neuronal Population. *Journal of Neuroscience*, 1988 8(8): p. 2928–2937. [PubMed: 3411362]
25. Kertzman C., et al., The role of posterior parietal cortex in visually guided reaching movements in humans. *Experimental Brain Research*, 1997 114(1): p. 170–183. [PubMed: 9125463]
26. Kettner RE., Schwartz AB., and Georgopoulos AP., Primate Motor Cortex and Free Arm Movements to Visual Targets in 3-Dimensional Space .3. Positional Gradients and Population Coding of Movement Direction from Various Movement Origins. *Journal of Neuroscience*, 1988 8(8): p. 2938–2947. [PubMed: 3411363]
27. Mirabella G., Pani P., and Ferraina S., Neural correlates of cognitive control of reaching movements in the dorsal premotor cortex of rhesus monkeys. *J Neurophysiol*, 2011 106(3): p. 1454–66. [PubMed: 21697448]
28. Pesaran B., Nelson MJ., and Andersen RA., Dorsal premotor neurons encode the relative position of the hand, eye, and goal during reach planning. *Neuron*, 2006 51(1): p. 125–34. [PubMed: 16815337]
29. Rubino D., Robbins KA., and Hatsopoulos NG., Propagating waves mediate information transfer in the motor cortex. *Nat Neurosci*, 2006 9(12): p. 1549–57. [PubMed: 17115042]
30. Scherberger H., Jarvis MR., and Andersen RA., Cortical local field potential encodes movement intentions in the posterior parietal cortex. *Neuron*, 2005 46(2): p. 347–354. [PubMed: 15848811]
31. Schwartz AB., Kettner RE., and Georgopoulos AP., Primate Motor Cortex and Free Arm Movements to Visual Targets in 3-Dimensional Space .1. Relations between Single Cell Discharge and Direction of Movement. *Journal of Neuroscience*, 1988 8(8): p. 2913–2927. [PubMed: 3411361]
32. Snyder LH., Batista AP., and Andersen RA., Coding of intention in the posterior parietal cortex. *Nature*, 1997 386(6621): p. 167–70. [PubMed: 9062187]
33. Takahashi K., et al., Encoding of Both Reaching and Grasping Kinematics in Dorsal and Ventral Premotor Cortices. *Journal of Neuroscience*, 2017 37(7): p. 1733–1746. [PubMed: 28077725]
34. Truccolo W., et al., Primary motor cortex tuning to intended movement kinematics in humans with tetraplegia. *J Neurosci*, 2008 28(5): p. 1163–78. [PubMed: 18234894]
35. Yanai Y., et al., Coordinate transformation is first completed downstream of primary motor cortex. *J Neurosci*, 2008 28(7): p. 1728–32. [PubMed: 18272693]
36. Zinger N., et al., Functional organization of information flow in the corticospinal pathway. *J Neurosci*, 2013 33(3): p. 1190–7. [PubMed: 23325255]
37. Shalit U., et al., Descending Systems Translate Transient Cortical Commands into a Sustained Muscle Activation Signal. *Cerebral Cortex*, 2012 22(8): p. 1904–1914. [PubMed: 21965441]
38. Isa T., Kinoshita M., and Nishimura Y., Role of direct vs. indirect pathways from the motor cortex to spinal motoneurons in the control of hand dexterity. *Frontiers in neurology*, 2013 4: p. 191. [PubMed: 24312077]
39. Alstermark B., et al., Motor command for precision grip in the macaque monkey can be mediated by spinal interneurons. *Journal of neurophysiology*, 2011 106(1): p. 122–126. [PubMed: 21511706]
40. Isa T., et al., Direct and indirect cortico-motoneuronal pathways and control of hand/arm movements. *Physiology*, 2007 22(2): p. 145–152. [PubMed: 17420305]

41. Pauvert V., Pierrot-Deseilligny E., and Rothwell J., Role of spinal premotoneurons in mediating corticospinal input to forearm motoneurons in man. *The Journal of physiology*, 1998 508(1): p. 301–312. [PubMed: 9490856]
42. Illert M. and Lundberg A., Collateral connections to the lateral reticular nucleus from cervical propriospinal neurones projecting to forelimb motoneurons in the cat. *Neuroscience letters*, 1978 7(2–3): p. 167–172. [PubMed: 19605107]
43. Alstermark B. and Ekerot CF., The lateral reticular nucleus: a precerebellar centre providing the cerebellum with overview and integration of motor functions at systems level. A new hypothesis. *The Journal of physiology*, 2013 591(22): p. 5453–5458. [PubMed: 24042498]
44. Alstermark B., et al., Integration in descending motor pathways controlling the forelimb in the cat. *Experimental Brain Research*, 1981 42(3–4): p. 282–298. [PubMed: 6263663]
45. Carmena JM., et al., Learning to control a brain-machine interface for reaching and grasping by primates. *PLoS Biol*, 2003 1(2): p. E42. [PubMed: 14624244]
46. Taylor DM., Tillery SIH., and Schwartz AB., Direct cortical control of 3D neuroprosthetic devices. *Science*, 2002 296(5574): p. 1829–1832. [PubMed: 12052948]
47. Pohlmeier EA., et al., Using Reinforcement Learning to Provide Stable Brain-Machine Interface Control Despite Neural Input Reorganization. *Plos One*, 2014 9(1).
48. MacDougall M., et al., Optogenetic manipulation of neural circuits in awake marmosets. *Journal of Neurophysiology*, 2016 116(3): p. 1286–1294. [PubMed: 27334951]
49. Prins NW., et al., Common marmoset (*Callithrix jacchus*) as a primate model for behavioral neuroscience studies. *Journal of neuroscience methods*, 2017 284: p. 35–46. [PubMed: 28400103]
50. Walker J., MacLean J., and Hatsopoulos NG., The marmoset as a model system for studying voluntary motor control. *Developmental Neurobiology*, 2017 77(3): p. 273–285. [PubMed: 27739220]
51. Burman KJ., et al., Anatomical and physiological definition of the motor cortex of the marmoset monkey. *Journal of Comparative Neurology*, 2008 506(5): p. 860–876. [PubMed: 18076083]
52. Chaplin TA., et al., A Conserved Pattern of Differential Expansion of Cortical Areas in Simian Primates. *Journal of Neuroscience*, 2013 33(38): p. 15120–15125. [PubMed: 24048842]
53. Prut Y. and Perlmutter SI., Firing properties of spinal interneurons during voluntary movement. I. State-dependent regularity of firing. *Journal of Neuroscience*, 2003 23(29): p. 9600–9610. [PubMed: 14573540]
54. Prut Y. and Perlmutter SI., Firing properties of spinal interneurons during voluntary movement. II. Interactions between spinal neurons. *Journal of Neuroscience*, 2003 23(29): p. 9611–9619. [PubMed: 14573541]
55. Alstermark B., Johannisson T., and Lundberg A., The inhibitory feedback pathway from the forelimb to C3-C4 propriospinal neurones investigated with natural stimulation. *Neurosci Res*, 1986 3(5): p. 451–6. [PubMed: 3018641]
56. Riddle CN. and Baker SN., Convergence of pyramidal and medial brain stem descending pathways onto macaque cervical spinal interneurons. *J Neurophysiol*, 2010 103(5): p. 2821–32. [PubMed: 20457863]

Highlights

- Spinal surgical techniques in marmosets are discussed in detail.
- Feasibility of establishing a spinal cord interface in marmosets is discussed.
- Electrophysiological data can be acquired in awake, chronic implants in marmosets

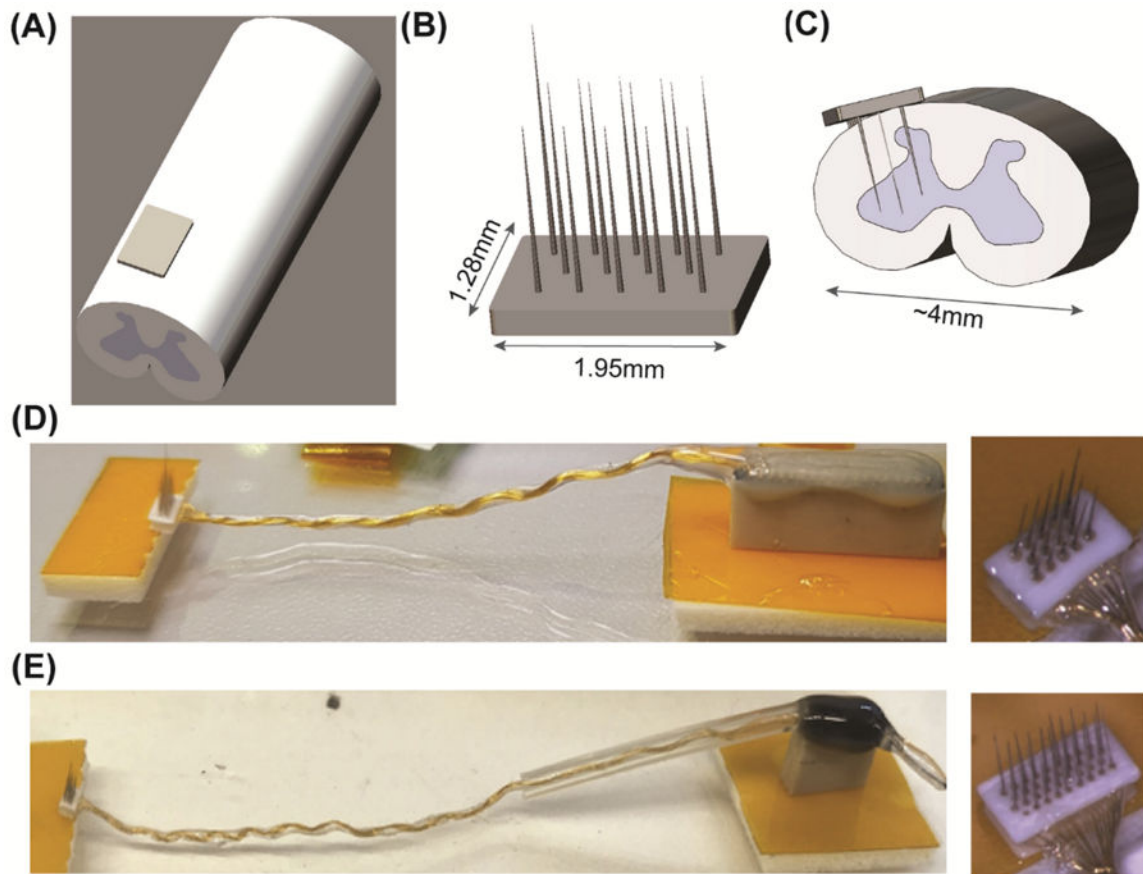
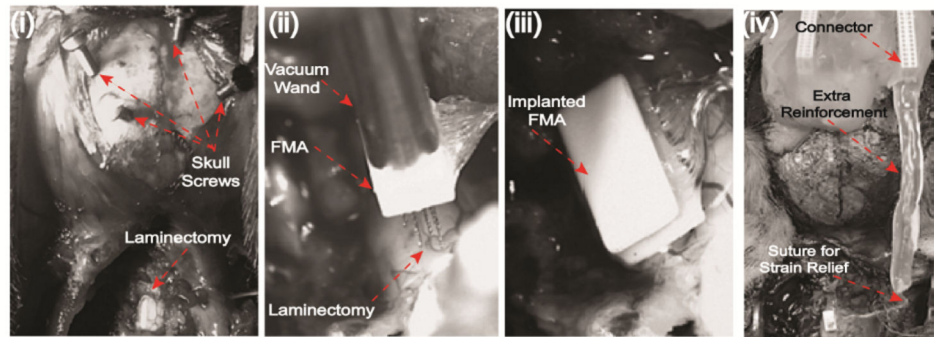


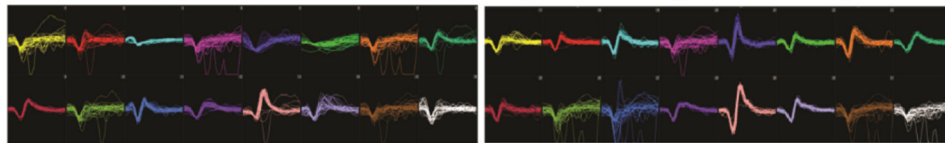
Figure 1: Floating microelectrode array (FMA) schematics for spinal implant.

(A) Electrode location along the rostrocaudal axis is shown on the spinal cord ipsilateral to the dominant forelimb of the animal (B) Schematic of a 13-channel FMA that were used in two implants. Each FMA (13 or 32-channel array) was connected to either a 16-channel or a 32-channel Omnetics connector using an interconnect cable. A 32-channel array had higher number of electrodes with the same inter-electrode distance of $250\mu\text{m}$. (C) A cross-section of the spinal cord is shown with the desired implant location. (D) 13-channel FMA is shown without the silicone sheath (E) 32-channel FMA is shown with the silicone sheath that was used to reinforce the interconnect wire.

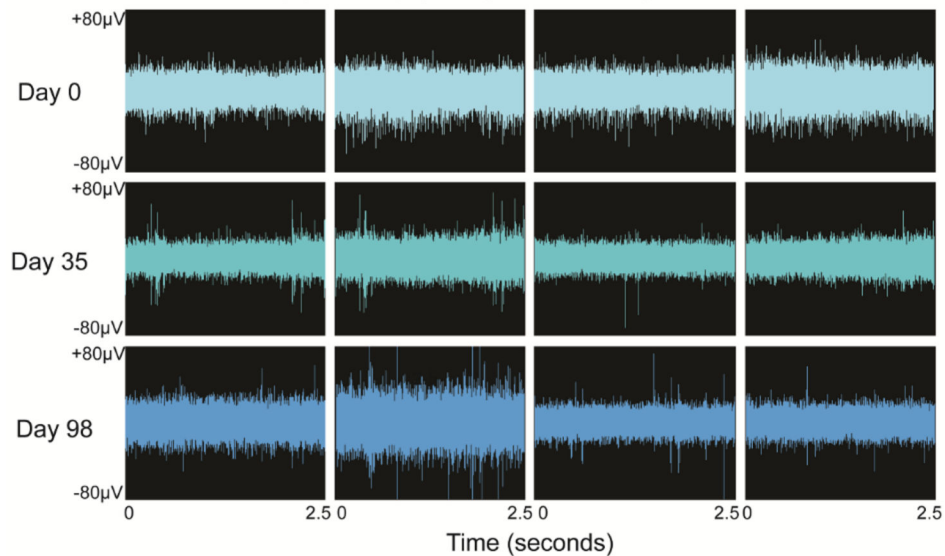
(A) Skull Preparation for Headstage Assembly, Laminectomy and FMA Implantation



(B) Intraoperative Electrophysiological Recordings (32 channels)



(C) Electrophysiological Recordings

**Figure 2: Surgical implantation of microelectrode array in the spinal cord:**

(A) *Skull preparation for headstage assembly, laminectomy, and FMA implantation:* (i) Laminectomy at C3-C4 was performed to expose the spinal cord and screw locations are shown on the skull that were used to anchor the omnetics microconnector on the head, (ii) The FMA was held using a vacuum wand attached to the stereotactic arm and stereotactically lowered into the spinal cord tissue, (iii) A 32-channel FMA is shown after it was stereotactically inserted in the cervical C3-C4 level of the spinal cord, (iv) After the FMA was implanted, a strain relief was provided to the interconnect cable. The image also shows the silicone reinforcement on the cable and the location of the connector on the skull with dental acrylic used to fix the connector. (B) *Intraoperative electrophysiological recordings:* Multi-unit activity from a 32-channel FMA that was acquired intraoperatively with manually set threshold levels. (C) *Electrophysiological recordings:* Four channels of broad band

activity recorded from the spinal cord, bandpass filtered between 500Hz-6kHz, are shown for day 0 (post-surgery) and at chronic time-points on days 35 and 98, respectively.

Author Manuscript

Author Manuscript

Author Manuscript

Author Manuscript

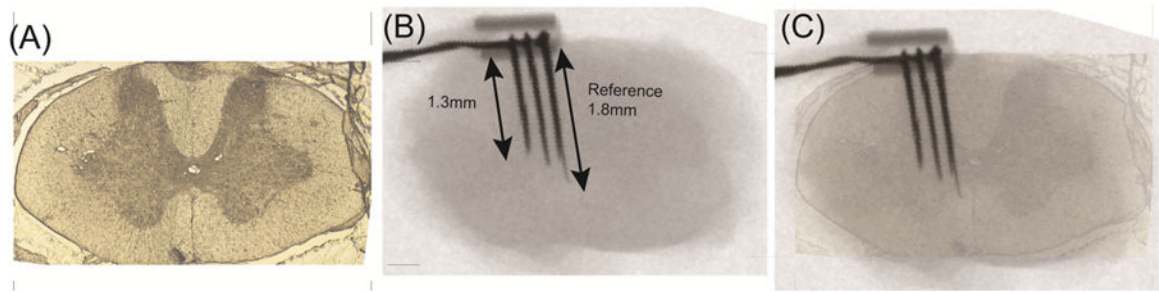


Figure 3: Post-mortem micro-CT imaging.

(A) Brightfield image of an intact marmoset spinal cord with no implant at the C3-C4 level
(B) micro-CT image with the microelectrode implant in the spinal cord (C) micro-CT image overlaid on the brightfield image of an unimplanted cord to show the location of the electrode tips relative to the spinal cord.

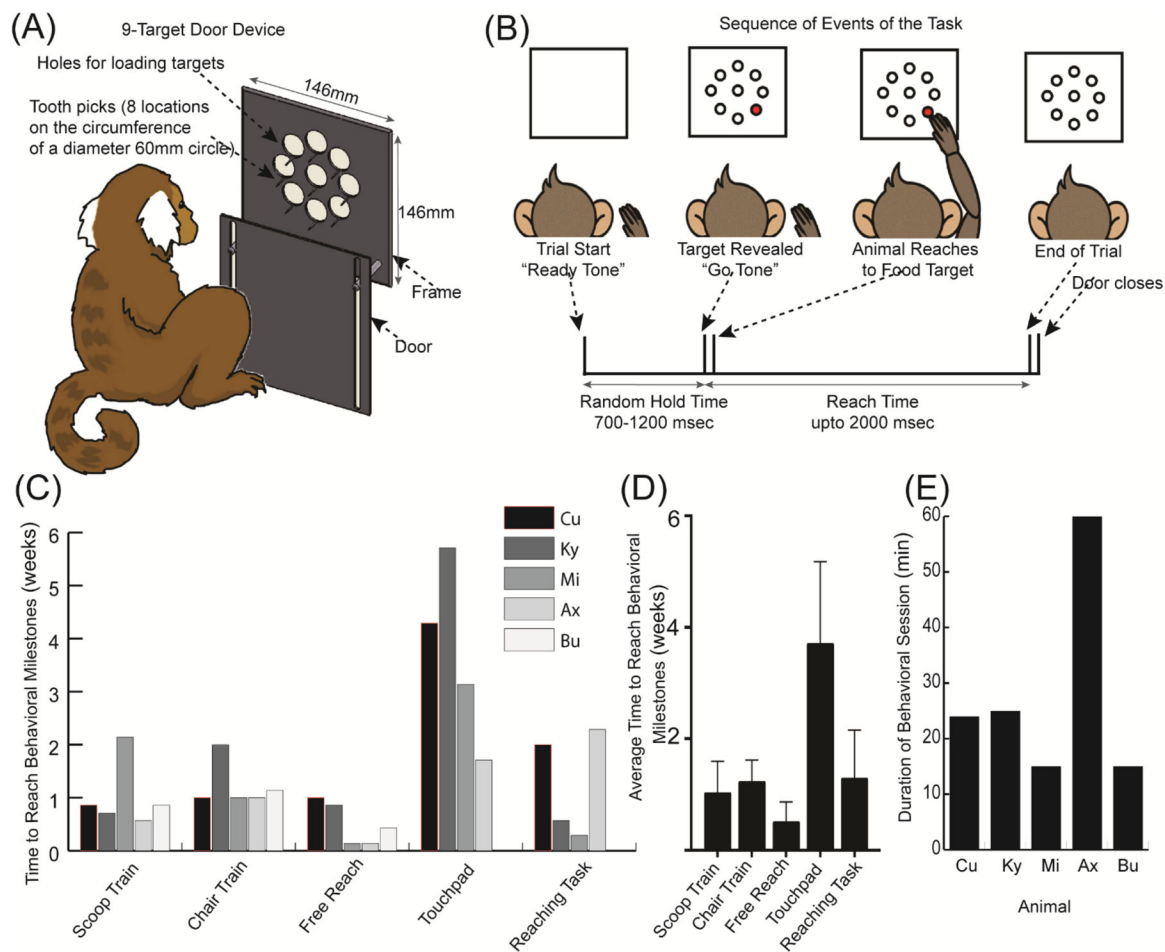


Figure 4: Behavioral task and training times:

(A) Animal with the 9-target door device in front of him (not to scale); (B) A sequence of the events of the task with timeline; (C) Individual times taken (in weeks) for 5 animals to reach behavioral milestones; (D) Mean and standard deviation of 5 animals trained for each behavioral milestone; (E) Approximate duration (minutes) for which each animal performed during a behavioral session.

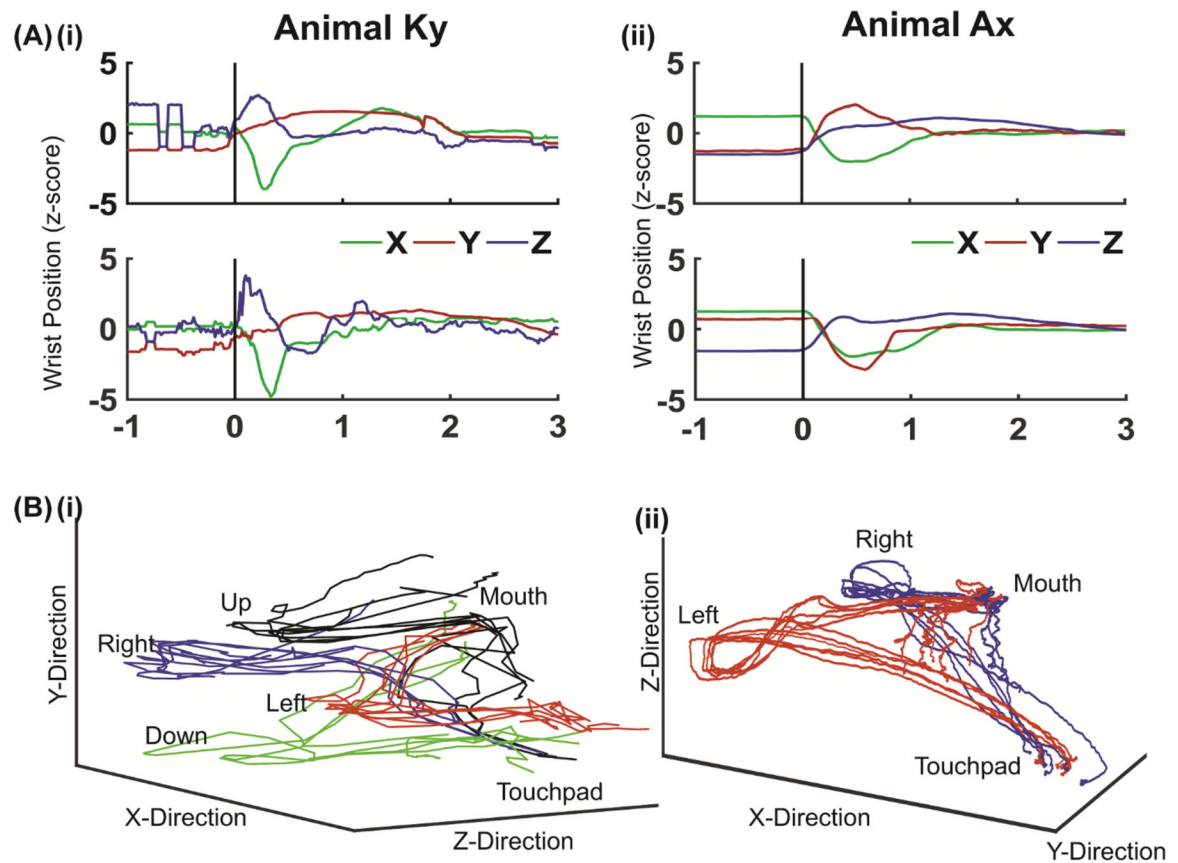


Figure 5: Kinematics and reconstructed 3D trajectories:

Two examples from two animals showing average wrist position in x, y and z directions.

Each subplot is an average of five trials towards one target. The black vertical line indicates movement onset. Trajectories from Ky were sampled at 60Hz with the MaxPRO system and those from Ax were sampled at 1017Hz with the trakstar system. The x, y and z directions are unique to the respective arm tracking systems. 3D trajectories of individual reaches from the respective systems are illustrated below the averages. Labels indicate the positions of the touchpad from which animals move their hands, the targets, and their mouth. Each direction is plotted in a different color.

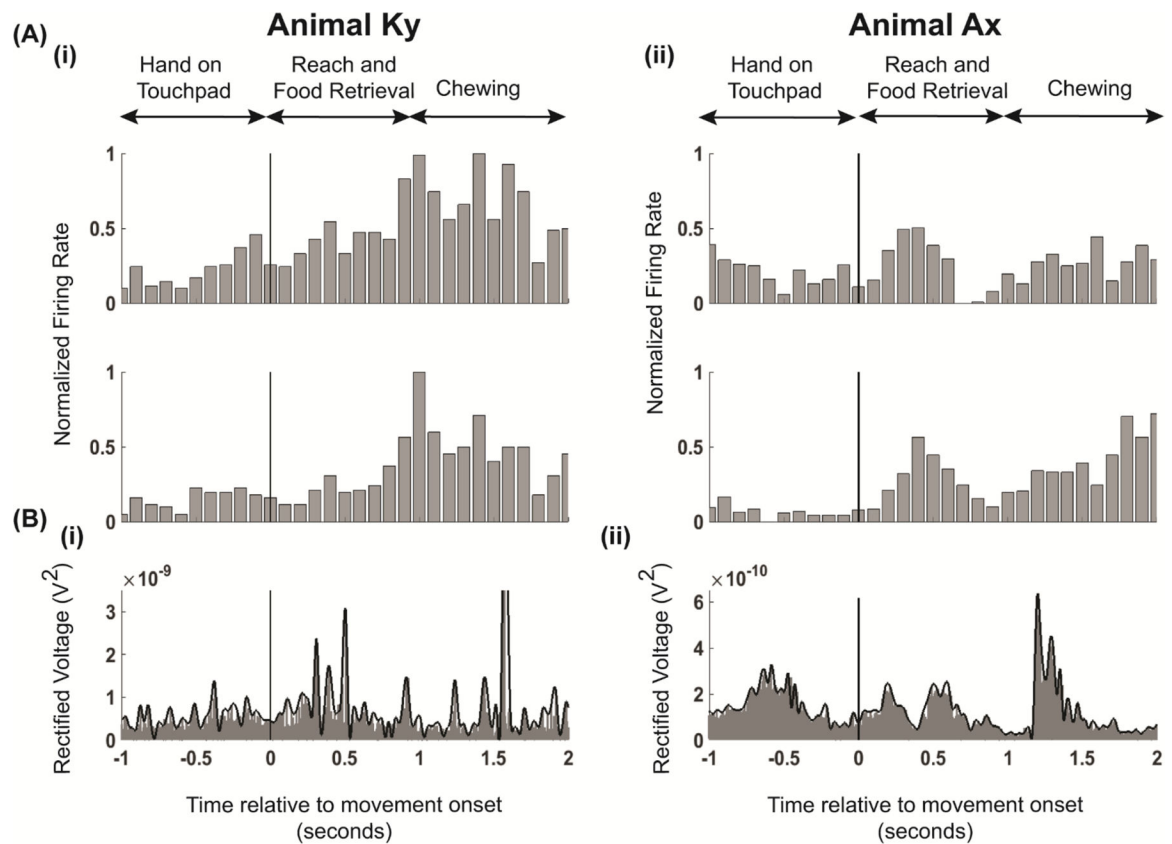


Figure 6: Neural data during behavioral reaching task.

(A) Two example channels of multiunit activity from two animals. Baseline activity is shown before movement onset (before zero, vertical black line) and increases with movement. Movement in y direction peaks at around 1 second (as seen in Figure 5) corresponding to the multiunit activity increase in both animals Ky and Ax. (B) Average of 32 Channels of broadband activity (500 – 6000 Hz) from animal (i) Ky and (ii) Ax during a trial. Though there is some variability during the phase prior to reaching, activity increases following movement onset during reach and retrieval (vertical black line). Black trace shows the positive peaks of the signal using the Matlab envelope function.

Table 1:

Summary of behavioral task, training and recording duration, and electrode failure mode

Animal	Behavior (Reaching Task)	~ # of trials/ training session	FMA Type (recording depths of 1.3 – 1.5 mm from dorsal surface)	Recording duration post- surgery (months)	Failure Mode
Cu	2-Target	100	32 - Channel	1.43	Mechanical failure (interconnect cable broke)
Mi		25	13 - Channel	3.97	Mechanical failure (interconnect cable broke)
Ky	9-Target	50	13- Channel	5.17	Signal degradation
Ax		200	32 - Channel	4.50	In study
Bu	Touch Screen	100	32 - Channel	1.67	Mechanical failure (interconnect cable broke)

Author Manuscript

Author Manuscript

Author Manuscript

Author Manuscript